

Absolute quantification of myosin heavy chain isoforms by selected reaction monitoring can underscore skeletal muscle changes in a mouse model of amyotrophic lateral sclerosis

Caterina Peggion¹ · Maria Lina Massimino² · Giancarlo Biancotto³ · Roberto Angeletti³ · Carlo Reggiani¹ · Maria Catia Sorgato^{1,2} · Alessandro Bertoli¹ · Roberto Stella³

Received: 5 October 2016 / Revised: 5 December 2016 / Accepted: 15 December 2016 / Published online: 11 January 2017
© Springer-Verlag Berlin Heidelberg 2017

Abstract Skeletal muscle fibers contain different isoforms of myosin heavy chain (MyHC) that define distinctive contractile properties. In light of the muscle capacity to adapt MyHC expression to pathophysiological conditions, a rapid and quantitative assessment of MyHC isoforms in small muscle tissue quantities would represent a valuable diagnostic tool for (neuro)muscular diseases. As past protocols did not meet these requirements, in the present study we applied a targeted proteomic approach based on selected reaction monitoring that allowed the absolute quantification of slow and fast MyHC isoforms in different mouse skeletal muscles with high reproducibility. This mass-spectrometry-based method was validated also in a pathological specimen, by comparison of the MyHC expression profiles in different muscles from healthy mice and a genetic mouse model of amyotrophic lateral sclerosis (ALS) expressing the *SOD1*(G93A) mutant. This analysis showed that terminally ill ALS mice have a fast-to-slow shift in the fiber type composition of the tibialis anterior and gastrocnemius muscles, as previously reported.

These results will likely open the way to accurate and rapid diagnoses of human (neuro)muscular diseases by the proposed method.

Keywords Selected reaction monitoring · Targeted proteomics · Absolute quantification · Amyotrophic lateral sclerosis · Myosin heavy chain · Skeletal muscle

Introduction

Skeletal muscles fulfill a variety of tasks by recruiting muscle fibers with specific functional properties. They are composed of distinct fiber types, originally classified on the basis of the ATPase and/or metabolic enzyme activity. The first classification into type I and type II fibers, proposed by Dubowitz and Pearse [1] in 1960, was followed by the identification of two fast-twitch fiber subtypes with specific metabolic properties [2–4]. Subsequently, differences in ATPase activity and pH sensitivity of fibers were found to depend on distinct myosin isoforms. Myosin, the most abundant myofibrillar protein in the skeletal muscle (it constitutes approximately 50% of the whole protein content) and the major determinant of the contractile performance, is made by multiple copies of two different proteins (named chains); that is, by two heavy chains and four light chains [5]. Combination of histochemistry, immunohistochemistry, and gel electrophoresis tools allowed the identification of four major myosin heavy chain (MyHC) isoforms in the trunk and limb striated muscles of mammals, indicated as I (or slow) and IIa, IIx, and IIb (or fast) [6, 7].

On the basis of the present genomic information, MyHC isoforms belong to a gene family composed of ten distinct genes [8]. In particular, fibers classified as type I express the type I MyHC isoform, whereas fibers classified as type IIa,

Electronic supplementary material The online version of this article (doi:10.1007/s00216-016-0160-2) contains supplementary material, which is available to authorized users.

✉ Alessandro Bertoli
alessandro.bertoli@unipd.it

✉ Roberto Stella
rstella@izsvenezie.it

¹ Department of Biomedical Sciences, University of Padua, Via Ugo Bassi 58/B, 35131 Padua, PD, Italy

² CNR Neuroscience Institute, University of Padua, Via Ugo Bassi 58/B, 35131 Padua, PD, Italy

³ Department of Chemistry, Istituto Zooprofilattico Sperimentale delle Venezie, Viale dell'Università, 10, 35020 Legnaro, PD, Italy

IIX, and IIB contain type IIa, IIx, and IIb MyHC isoforms [6]. Although many fibers contain only a single MyHC isoform (the so-called pure fibers) [9], two or more different MyHC isoforms can be coexpressed in the same fiber (e.g., in the extraocular muscle fibers [10]), which are called hybrid fibers [11]. Different mammalian species (e.g., human, mouse, rat, rabbit, and guinea pig) show similar skeletal muscle fiber type profiles; the type IIb MyHC isoform, however, is not detectable in humans and in several other mammalian species, despite the presence of the corresponding gene [12].

An important characteristic of skeletal muscles is plasticity, which indicates the ability to adapt the fiber type composition to prevailing pathophysiological conditions [13]. Modification of the muscle fiber profile may thus depend on factors such as exercise, hormonal signaling (e.g., by thyroid hormones, glucocorticoids, testosterone, or β -agonists), and nutrient availability (e.g., fasting or high-fat diet), but also on pathological conditions, including diabetes, Duchenne muscular dystrophy [14], amyotrophic lateral sclerosis (ALS) [15, 16], congenital fiber type disproportion [17], and myosinopathies caused by mutations in MyHC genes [18].

Under these premises, evaluation of the skeletal muscle fiber type/MyHC composition clearly necessitates easy-to-perform assays, capable of bypassing the laborious myofiber discrimination based on the ATPase activity [19, 20], or the time-consuming immunohistochemistry of contiguous muscle cryosections using monoclonal antibodies to different MyHCs [21, 22]. Gel-based methods have successfully reduced the assay time by allowing the simultaneous detection of different MyHC isoforms, whereas Western blot (WB) has also allowed comparison of selected MyHC isoforms in different muscle samples. However, the similar masses of MyHC isoforms have hindered their efficient discrimination by conventional sodium dodecyl sulphate (SDS)–polyacrylamide gel electrophoresis (PAGE). Although improved electrophoretic protocols have been developed [23–27], they still suffer from poor reproducibility, lengthy (24–42 h) electrophoretic runs, and uncertain discrimination of MyHC isoforms (e.g., for mouse type IIa MyHC and type IIx MyHC) in standard mini-gel systems [28].

Thus, to determine precisely the content of MyHC isoforms in different mouse skeletal muscles, in this study we have used a method comprising a targeted proteomic approach based on liquid chromatography coupled with tandem mass spectrometry (LC–MS/MS), and selected reaction monitoring (SRM). We found that the data on muscle fiber composition obtained with this approach were similar to those reported in the literature. However, by inclusion of the SRM technique, which quantifies MyHC-isoform-specific peptides, the whole procedure had the great advantage of accomplishing absolute quantification of the different MyHC isoforms, and increasing reproducibility by analyzing tens of samples in the same analytical session.

We also assessed the applicability of the proposed method to the pathological context of ALS. ALS is a progressive and fatal neurodegenerative disorder characterized by the selective injury and death of motor neurons in the spinal cord, brainstem, and cerebral cortex [29, 30]. Twenty percent of familial ALS cases (which account for 10% of total ALS cases) are associated with mutations in the gene encoding the cytosolic antioxidant enzyme Cu/Zn superoxide dismutase 1 (SOD1) [31]. Transgenic (Tg) mice are now available that overexpress the *SOD1(G93A)* missense mutant, closely reproducing human ALS [32]. The long-standing view of ALS affecting only motor neurons has been challenged recently by the finding that non-neuronal cells, including skeletal muscle fibers, play an active role in disease pathogenesis [33, 34]. Accordingly, severe skeletal muscle alterations occur in ALS patients and animal models [16, 35, 36].

In light of these notions, we applied the SRM-based approach to evaluate the content of MyHC isoforms in skeletal muscles with different contractile properties, obtained from control mice and Tg-G93A mice at the terminal stage of the disease. The finding that some (i.e., tibialis anterior and gastrocnemius) fast muscles of ALS model mice showed a switch toward slow myofibers, as previously reported [15], strongly supports applicability of the proteomic approach presented here also to (neuro)muscular diseases.

Materials and methods

Animals, tissue sampling, and homogenization

We used C57BL6/J wild-type (WT) mice and B6SJL-Tg(SOD1-G93A)1Gur (Tg-G93A) and B6SJL-Tg(SOD1)2Gur/J (Tg-WT) Tg mice, overexpressing human *SOD1(G93A)* or *SOD1(WT)* respectively. All mouse strains were purchased from Jackson Laboratories. The mice were housed in a temperature-controlled (22 °C) SPF room with a 12 h–12 h light–dark cycle, and *ad libitum* access to food and water. All aspects of animal care and experimentation were performed in compliance with European and Italian (D.L. 116/92) laws concerning the care and use of laboratory animals. The authors' institution has been accredited for the use of experimental mice by the Italian Ministry of Health, and by the Ethical Committee of the University of Padua.

Only male mice were used to minimize individual biological variability. Mice were anesthetized by CO₂ just before they were killed by cervical dislocation at 120 days after birth, an age at which, after progressive motor neuron degeneration, severe muscle atrophy and paralysis occur in Tg-G93A mice, indicating the terminal stage of illness. Age-matched WT mice and Tg-WT mice do not show any overt phenotype.

The diaphragm and four morphological distinct hindlimb muscles were explanted for analysis: the mixed fast-twitch extensor digitorum longus, tibialis anterior, and medial gastrocnemius, and the slow-twitch soleus. A single liver sample was also collected for the generation of calibration curves (see later). Tissues were immediately frozen in liquid nitrogen, and stored at $-80\text{ }^{\circ}\text{C}$ for subsequent analyses.

Protein extracts were obtained by homogenization of tissues with 10 vol of lysis buffer [62.5 mM tris(hydroxy methyl)aminomethane-HCl (pH 6.8), 10% (w/v) glycerol, 2.3% (w/v) SDS, and protease inhibitors (Roche, Basel, Switzerland)]. After centrifugation (16,000 g, 10 min, $4\text{ }^{\circ}\text{C}$) to remove tissue debris, protein concentration was determined by a bicinchoninic acid based assay kit (Thermo Scientific, Waltham, MA, USA).

Immunofluorescence-based fiber typing

Muscles cross-sections (10 μm thick) were cut in a cryostat ($-24 \pm 2\text{ }^{\circ}\text{C}$) (Leica CM1850). To examine the overall muscle morphology, cryosections of each analyzed muscle were hematoxylin-eosin stained as described previously [37]. To determine the fiber type composition, cryosections were co-immunostained (30 min, $37\text{ }^{\circ}\text{C}$), with an anti-laminin rabbit polyclonal antibody [Sigma, St Louis, MO, USA, catalog no. L9393; diluted 1:100 in phosphate-buffered saline (PBS) containing 1% (w/v) bovine serum albumin (BSA) (PBS-BSA)], and with each of the following anti-MyHC mouse monoclonal antibodies (diluted 1:10 in PBS-BSA): clone BA-D5, which recognizes type I MyHC, clone SC-71 for type IIa MyHC, and clone BF-35 for type I, IIa, and IIb MyHC (all from the Developmental Studies Hybridoma Bank, University of Iowa). After the sections had been washed with PBS, they were incubated (30 min, $37\text{ }^{\circ}\text{C}$) with tetramethylrhodamine isothiocyanate conjugated anti-rabbit and Alexa Fluor 488 conjugated anti-mouse secondary antibody (Molecular Probes, Eugene, OR, USA, diluted 1:400 in PBS-BSA). After a final rinse with PBS, fluorescently labeled sections were mounted on a glass slide with use of a mounting solution [8% (w/v) Mowiol 40-88 (Sigma) in a solution of glycerol 25% (v/v) in PBS] and observed with an inverted fluorescence microscope (CTR6000, Leica, Wetzlar, Germany) equipped with a computer-assisted charge-coupled camera (Hamamatsu Orca flash 4.0). Images of different fields from each section were digitized and stored for subsequent analysis. Type I, IIa, and IIb MyHC immunopositive fibers were counted and expressed as the percentage of total laminin-positive fibers. The laminin-positive fibers not stained by the BF-35 antibody were considered as type IIX fibers.

SDS-PAGE and WB analysis

To analyze MyHC isoforms, muscle proteins were diluted to the desired final protein concentration with lysis buffer supplemented with bromophenol blue [final concentration (f.c.), 0.02% (w/v)], and separated by SDS/glycerol-PAGE according to the modified method of Talmadge and Roy [23], as previously reported [38]. The total amount of proteins loaded in each lane was 0.8 μg . Gels were then subjected to silver staining according to standard procedures [39], or to WB analysis as described below. For the densitometric analysis of silver-stained bands, gel images were digitalized by means of a high-resolution scanner, and the band intensity of each MyHC isoform—calculated by the Kodak 1D image analysis program—was normalized to the total intensity of all MyHC isoforms detected in the muscle sample.

To assess myogenin expression levels, proteins were diluted to the desired final protein concentration with lysis buffer supplemented with dithiothreitol (f.c., 50 mM) and bromophenol blue [f.c., 0.02% (w/v)], and boiled (5 min). SDS-PAGE was performed with Mini-Protean TGX precast gels [4–15% acrylamide-bisacrylamide (Bio-Rad Laboratories, Hercules, CA, USA)], with 20 μg of total proteins loaded per lane.

For WB, proteins were electrophoretically transferred onto poly(vinylidene difluoride) membranes (1 h, 350 mA), which were then stained with Coomassie brilliant blue (Sigma) to ensure equal protein loading and transfer. After they had been destained with methanol, membranes were incubated (1 h, room temperature) in a blocking solution [5% (w/v) non-fat dry milk (Bio-Rad Laboratories) in PBS to which 0.1% (w/v) Tween 20 (PBS-T) was added]. Membranes were then incubated (overnight, $4\text{ }^{\circ}\text{C}$) with the desired primary antibody diluted in blocking solution (see below), washed three times with PBS-T, and then incubated (1 h, room temperature) with horseradish peroxidase conjugated anti-mouse or anti-rabbit IgG secondary antibody (Santa Cruz Biotechnology, Dallas, TX, USA, catalog no. sc-2004 or sc-2005 respectively) diluted (1:3000) in blocking solution, according to the primary antibody.

The antibodies used were as follows (dilutions in parenthesis): anti-type I MyHC mouse monoclonal antibody (clone BA-D5, 1:5000); anti-type IIa MyHC mouse monoclonal antibody (clone SC-71, 1:1000); anti-type IIb MyHC mouse monoclonal antibody (clone F3, 1:5000); anti-type IIa and type IIX MyHC mouse monoclonal antibody (clone BF-13, 1:5000); and anti-myogenin rabbit polyclonal antibody (Santa Cruz Biotechnology, catalog no. sc-576, 1:2000). All anti-MyHC antibodies were from the Developmental Studies Hybridoma Bank, University of Iowa.

Immunoreactive bands were visualized and digitalized by means of a digital Kodak Image Station, with use of an enhanced chemiluminescence reagent kit (EMD Millipore, Billerica, MA, USA). For densitometric analyses, the intensity

of each immunoreactive band was normalized to the optical density of the corresponding lane stained with Coomassie blue.

Sample processing for LC–MS/MS

Protein extracts (50 μg , 20 μl) were processed with the filter-aided sample preparation (FASP) method [40], with use of a FASPTM protein digestion kit (30,000 molecular weight cutoff filters, Expedeon, San Diego, CA, USA), following the manufacturer's instructions. During sample processing, cysteines were reduced by addition of 100 μl dithiothreitol (f.c., 20 mM; 45 min, 55 °C), and then alkylated by addition of 100 μl iodoacetamide (f.c., 55 mM; 45 min, room temperature). Immediately before digestion, a solution (10 μl , 25 pmol) of isotopically labeled (¹³C₆, ¹⁵N₄-Arg or ¹³C₆, ¹⁵N₂-Lys) synthetic (heavy) peptides (JPT Peptides, Berlin, Germany) having the same sequence of the target peptides (two different peptides for each MyHC isoform analyzed) was added to the protein extracts as an internal standard. Subsequently, trypsin (Promega, Madison, WI, USA) was added (90 μl in 25 mM NH₄HCO₃) to a final enzyme-to-protein ratio of 1:25 (w/w), and protein digestion was performed overnight (37 °C). To recover protein digests, FASP filters were finally centrifuged (14,000 g, 10 min) and eluted peptides were collected. The filters were then rinsed with 50 μl of 25 mM NH₄HCO₃, and after centrifugation, the eluted residual peptides were added to the previous eluate.

Peptide solutions were acidified by addition of formic acid until pH ≤ 3 was reached, and then desalted with use of C₁₈ spin columns (The Nest Group, Southborough, MA, USA), following the manufacturer's instructions, with the exception that two sequential elution steps—with a solution (100 μl) containing acetonitrile (70% v/v) and formic acid (0.1% v/v)—were performed. Finally, peptide extracts were dried under vacuum and, immediately before LC–MS/MS analyses, dissolved in a solution (100 μl) containing acetonitrile (5% v/v) and formic acid (0.1% v/v) to obtain a final protein digest concentration of 0.5 $\mu\text{g } \mu\text{l}^{-1}$. Each protein digest was analyzed by two independent LC–MS/MS runs.

LC–MS/MS analysis and SRM

The mass spectrometry data have been deposited in the PASSEL repository (<http://www.peptideatlas.org/PASS/PASS00887>; dataset identifier PASS00887; password QE7545ha). Peptides were analyzed with an LC–MS/MS system operating in scheduled SRM mode. A Prominence high-performance liquid chromatography system (Shimadzu, Kyoto, Japan), interfaced with an API 4000 triple-quadrupole mass spectrometer (AB Sciex, Framingham, MA, USA) was used. The mass

spectrometry source parameters were as follows: ion spray voltage, 5000 V; source temperature, 500 °C; curtain gas, 15 psi; gas 1 and gas 2, 35 psi. The chromatographic separation was achieved with a Brownlee SPP peptide ES-C₁₈ column (100 mm \times 2.1 mm, 2.7 μm , PerkinElmer, Waltham, MA, USA), with injection of 10 μl of sample—corresponding to 5 μg of digested proteins—for each analysis, and with a flow rate of 0.3 ml min⁻¹. The elution solvents were 0.1% (v/v) formic acid (solvent A) and 0.1% (v/v) formic acid in acetonitrile (solvent B). The mobile phase composition was as follows: 97.5% solvent A and 2.5% solvent B from 0 to 1 min; 75% solvent A and 25% solvent B after 12 min (following a linear gradient); 30% solvent A and 70% solvent B after 14 min; 5% solvent A and 95% solvent B after 15 min; unchanged for 1 min; and finally 97.5 solvent A and 2.5% solvent B from 16.25 to 20 min to reequilibrate the system.

The scheduled SRM method was optimized with use of synthetic peptides to record the retention time and to select five diagnostic precursor-to-product ion transitions for each target peptide. The instrumental settings used in the acquisition method are reported in Table S1.

A seven-point calibration curve was built with unlabelled purified peptides (SpikeTidesTQTM, JPT Peptides), which were subjected to trypsin digestion and desalting as described earlier, in the presence of 25 pmol of labeled peptides. This procedure was performed in the presence of mouse liver homogenate (10 μg) to mimic the matrix effect exerted by protein extracts. The concentration ranges of the calibration curves for each MyHC isoform are reported in Table S1.

Five transitions, and the corresponding retention time, were used to assign the correct identity to the monitored peptides. Quantification was achieved with the peptide absolute quantification method [41]. The calibration curve for each peptide was obtained by calculation of the ratio between the area under the curve (AUC) of the peptide and the AUC of the corresponding labeled internal standard. Peptide concentrations were then calculated by a weighted linear regression of the calibration curve with use of Skyline (<https://skyline.gs.washington.edu/labkey/project/home/begin.view> [42]). Protein amounts, expressed as femtomoles per microgram of total protein digest, were finally determined by calculation of the mean concentration of the two monitored peptides for each MyHC isoform, and then by averaging of the values obtained from the two LC–MS/MS replicates.

The performance characteristics of the method were evaluated by analysis of a single protein extract from each different muscle in three independent working sessions, which allowed calculation of the coefficient of variation (CV;

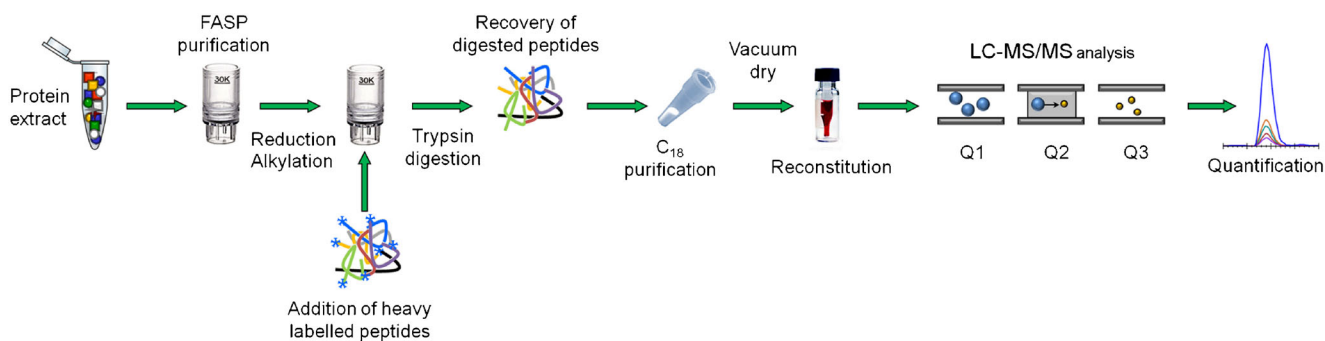


Fig. 1 Workflow of sample preparation and analysis for the quantification of myosin heavy chain (MyHC) isoforms in muscle protein extracts using the proposed liquid chromatography—tandem

mass spectrometry (*LC-MS/MS*)-based selected reaction monitoring (SRM) technique (see “Materials and methods”). *FASP* filter-aided sample preparation

defined as the percentage ratio of the standard deviation and the mean value) for each muscle and each MyHC isoform.

Experimental design and statistical rationale

To avoid confusing effects from biological variability, the validation of the SRM method was performed by assessing the technical variability on muscle samples from a single WT mouse. In this case, three peptide digests prepared in distinct working sessions were analyzed in two different LC–MS/MS runs, yielding six independent technical replicates.

For comparative analyses on Tg-G93A mice and Tg-WT mice, muscles were isolated from three different mice for each genotype. A single protein extract from each muscle was then processed for peptide digestion and purification, and analyzed in two distinct LC–MS/MS runs.

All data are presented as the mean \pm standard error of the mean. Statistical comparisons were performed with the unpaired Student’s *t* test, $p < 0.05$ being considered statistically significant.

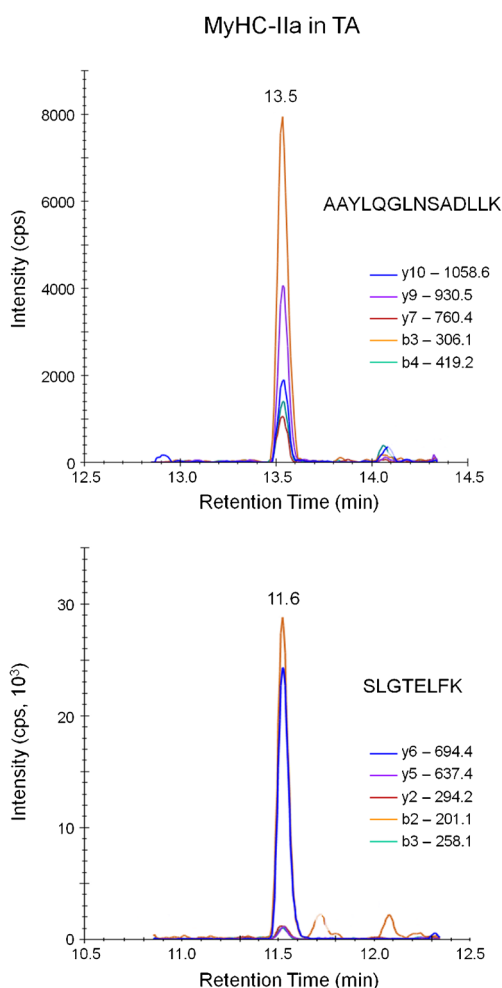


Fig. 2 SRM transition signals and signal-to-noise ratio for the tibialis anterior (TA) muscle type IIa MyHC. Representative SRM chromatograms relative to five diagnostic transitions of the two monitored peptides for type IIa MyHC (amino acid sequences are reported in each panel) in the tibialis anterior muscle. Although type IIa MyHC is present at low concentration in the tibialis anterior muscle, both peptides show a clear signal, and a signal-to-noise ratio greater than 3, for all the selected transitions, indicated in the *inset* in each plot

Results

We have developed a targeted proteomic approach allowing the absolute quantification of slow (type I) and fast (type IIa, IIb, and IIx) MyHC in skeletal muscles. This study used SRM, which has been proven to be optimally suited for quantifying proteins [43–46], by repeatedly targeting and detecting the same set of peptides in different samples through a triple-quadrupole mass spectrometer.

Peptides from different muscles (i.e., extensor digitorum longus, tibialis anterior, medial gastrocnemius, soleus, and diaphragm) were obtained after the tryptic digestion of muscular protein samples (extracted with an SDS-containing buffer) and purified through a FASP protocol (Fig. 1). For each MyHC isoform, two proteotypic peptides (8–14 amino acid long) [47, 48] were selected as standards for SRM measurements (Table S1) on the basis of their unique presence in a single MyHC and insusceptibility to artificial modifications (they do not contain methionines or cysteines) or to incomplete cleavage. Five

precursor-to-product ion transitions for each peptide were carefully chosen to provide optimal signal intensity, thereby allowing us to easily distinguish the target peptide from other molecules. An example of such an optimized selection of the transitions is reported in Fig. S1.

The absolute quantification method was used to quantify each peptide abundance. To achieve more accurate measurements, each muscle protein sample was spiked with stable-isotope-labeled (heavy) synthetic peptides—corresponding to the target peptides—at a known concentration before trypsin digestion. Being chemically equivalent to and having the same ionization efficiency and fragmentation behavior as muscle-derived MyHC (light) peptides, heavy peptides allow correction for any putative peptide loss during the multistep preparation of the samples for LC–MS/MS analysis and for contaminating peptides that may be coeluted with the target peptides. Finally, the absolute quantification of each MyHC was achieved by calculation of the AUC ratio of light and heavy peptides and by use of a calibration curve. A peptide was considered undetectable if its concentration was below the lowest calibration point (i.e., 25, 10, 25, and 50 fmol μg^{-1} for isoforms I, IIa, IIx, and IIb respectively; see Table S1). Accordingly, an MyHC isoform was considered not quantifiable if one of the two monitored peptides was undetectable.

We ascertained that this method was sensitive enough to quantifying the selected MyHC isoform even if it was present at very low levels. An example is provided by the low-abundance type IIa MyHC in the tibialis anterior, whose AUC signal-to-noise ratio was greater than 3 (Fig. 2), and the concentration (23 ± 1 fmol μg^{-1}) was above the lowest calibration point (Fig. 3a).

The accuracy of the method was evaluated by calculation of the CV of MyHC concentrations in a single protein extract from each extensor digitorum longus, tibialis anterior, gastrocnemius, soleus, or diaphragm muscle during three distinct analytical sessions (Table 1), providing an average CV of less than 10% for the different MyHCs in the different muscles. In addition, linearity of the calibration curve for each MyHC was verified by calculation of the correlation coefficient (r), which optimally was greater than 0.99 for all MyHCs in all analytical sessions (Fig. S2). Taken together, these parameters establish the reliability of the SRM-based method for the absolute quantification of the MyHC composition of skeletal muscles.

It is important to note that, besides the good agreement of the SRM-based results (Fig. 3a, b) and data obtained from SDS–PAGE and silver nitrate staining of muscles (Fig. 3c, d), the major advantages of the SRM approach

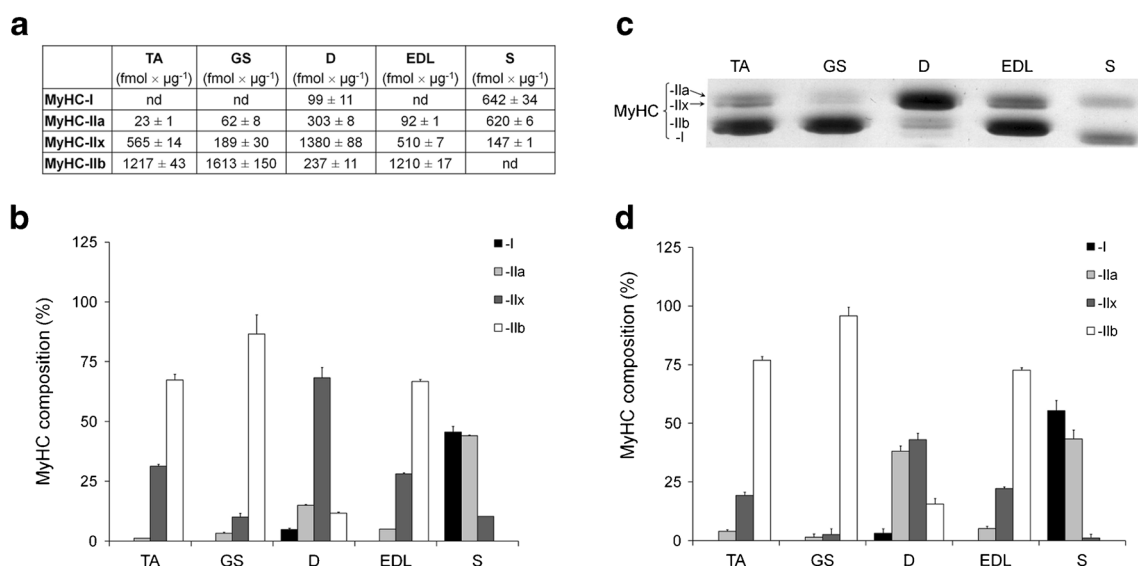


Fig. 3 Comparable quantification of MyHC isoforms by SRM-based and gel-electrophoresis-based approaches in muscle samples. **a**, **b** Protein extracts from the tibialis anterior (TA), gastrocnemius (GS), soleus (S), diaphragm (D), and extensor digitorum longus (EDL) muscles of a C57BL/6J wild-type male mouse were subjected to processing and SRM-based quantification of MyHC types I, IIa, IIx, and IIb, as described in “Materials and methods.” The absolute concentration of each MyHC isoform is reported in **a**, and **b** reports the relative MyHC composition of the different muscles, expressed as a percentage of the total MyHC amount measured in each muscle. **c**, **d** The same muscle samples analyzed by SRM in **a** and **b** were subjected to sodium dodecyl sulfate–polyacrylamide gel electrophoresis (SDS-

PAGE)-based protein separation (0.8 μg of total proteins per sample), followed by silver staining of gels and densitometric analysis of the MyHC bands. **c** A representative gel of three technical replicates. **d** Densitometric analysis of the different MyHC bands in the different muscles, expressed as a percentage of the total optical density of all MyHCs in each muscle. Although the closely matching molecular weight hampers the gel-based discrimination of type IIa MyHC and type IIx MyHC (**c**), the relative quantification of MyHCs obtained with the two methods provides comparable results (**b**, **d**). The reported values are the mean \pm standard error of the mean (SEM); six technical replicates in **a** and **b**, three technical replicates in **c** and **d**. nd not detectable

include the direct quantitative comparison of a given MyHC isoform in different muscles, and a clear identification of MyHC isoforms of similar mass, which, conversely, can hardly be achieved by gel-based techniques. The latter aspect could account for some discrepancy in the relative determination of type IIa MyHC-IIa and type IIx MyHC content by the two experimental procedures (Fig. 3b, d). The total MyHC content, calculated as the sum of each MyHC content reported in Fig. 3a, ranges between 1.8 and 2 pmol μg^{-1} . Assuming a molecular weight close to 200,000 Da, this means that MyHCs represent almost 40% of the total protein complement, a result very similar to that recently obtained with a different proteomic approach on mouse single muscle fibers (i.e., 30–35% [49]).

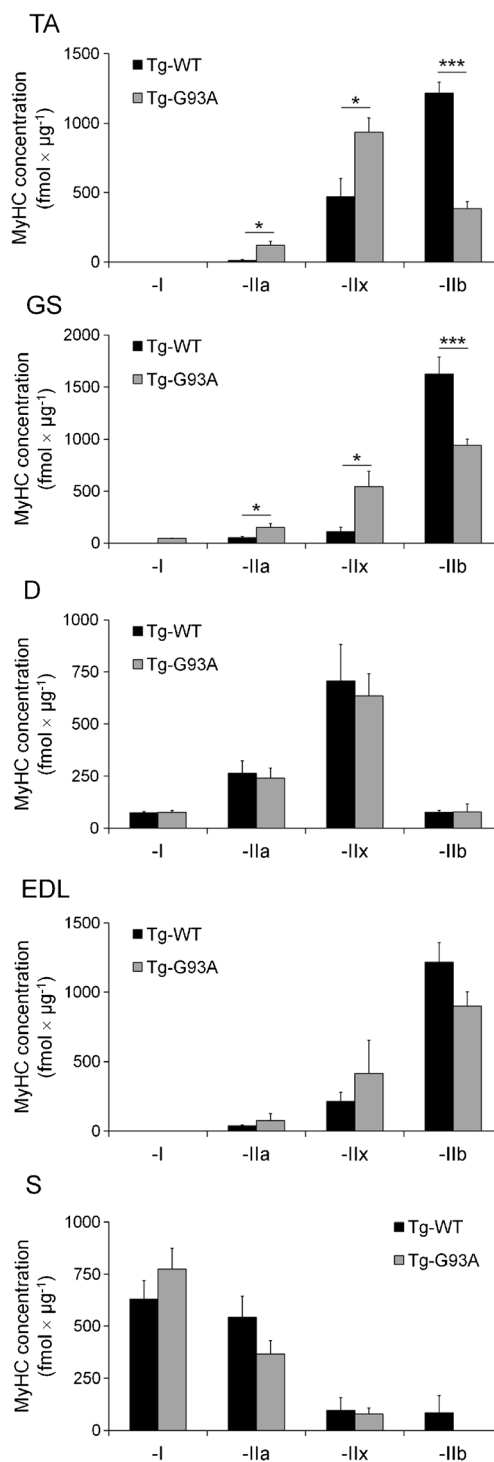
A key test for the wide use of the SRM-based method was its applicability to skeletal muscle diseases. We chose ALS, given some previous data pointing to alterations of muscle fiber type composition in this disease [15]. For this purpose, we compared MyHC expression profiles in four hindlimb muscles (extensor digitorum longus, tibialis anterior, gastrocnemius, and soleus) and in the diaphragm of terminally ill Tg-G93A mice (a widely accepted ALS model) and age-matched Tg-WT mice. As reported in Fig. 4 and Table S2, tibialis anterior and gastrocnemius muscles of Tg-G93A mice showed a significant decrease in the amount of type IIb MyHC (by 68% and 42% respectively), and a concomitant increase in the amount of type IIa MyHC (by 90% and 66% respectively) and type IIx MyHC (by 50 and 78% respectively) with respect to healthy mice, suggesting a fast-to-slow fiber transition in such muscles of ALS mice. Conversely, no significant alteration in the MyHC expression pattern was observed in extensor digitorum longus, soleus, or diaphragm muscles.

To confirm the SRM-based evaluation of MyHC expression in the tibialis anterior, gastrocnemius, and soleus muscles, we analyzed this parameter using conventional

Table 1 Coefficient of variation for the different myosin heavy chain (*MyHC*) isoforms in the murine skeletal muscles studied. Samples of the different skeletal muscles from a single C57BL/6/J wild-type mouse were processed and analyzed as described in the text. The reported coefficients of variation were calculated as the ratio of the standard deviation to the mean concentrations measured during the validation study, and are expressed as a percentage

MyHC type	TA	GS	D	EDL	S
I	ND	ND	19.5%	ND	9.2%
IIa	5.1%	21.1%	4.7%	2.2%	1.7%
IIx	4.4%	16.1%	11.1%	2.4%	1.0%
IIb	6.2%	27.4%	7.8%	2.5%	ND

D diaphragm, EDL extensor digitorum longus, GS gastrocnemius, ND not detectable, S soleus, TA tibialis anterior



gel-based SDS-PAGE and silver nitrate staining, and WB using specific antibodies recognizing MyHC type I, type IIb, type IIa, or both type IIa and type IIx. As shown in Figs. 5 and 6, both approaches provided results similar to those obtained with proteomics. Immunohistochemistry of cryosections of tibialis anterior muscle, which is the muscle most affected by the fast-to-slow fiber transition in ALS mice [15], further confirmed the data acquired by

Fig. 4 The SRM approach underscores remarkable differences in the MyHC expression profiles of fast-twitch muscles between healthy and end-stage amyotrophic lateral sclerosis mice. The absolute concentration of type I, IIa, IIx, and IIb MyHC in the tibialis anterior (TA), gastrocnemius (GS), diaphragm (D), extensor digitorum longus (EDL), and soleus (S) muscles of 4-month-old transgenic SOD1 (wild-type) (Tg-WT) and transgenic SOD1 (G93A) (Tg-G93A) male mice was assessed by the SRM-based method. The fast-twitch tibialis anterior and gastrocnemius muscles from terminally ill Tg-G93A mice show a significant reduction of the amount of type IIb MyHC, and a concomitant increase of the amount of type IIa and type IIx MyHC with respect to the Tg-WT counterpart. A similar trend occurs in the fast extensor digitorum longus muscle, although the differences do not reach statistical significance, whereas no difference is observed in the diaphragm and soleus. The reported values are the mean \pm SEM; three biological replicates. One asterisk $p < 0.05$, three asterisks $p < 0.005$, Student's t test

the SRM-based method (Fig. S3). Finally, because the myogenic helix-loop-helix transcription factor myogenin is more abundant in slow-twitch fibers than in fast fibers [50], tibialis anterior and gastrocnemius muscles of the aforementioned ALS and control mice were analyzed (by WB) for myogenin expression. The finding that both Tg-G93A muscles exhibited increased myogenin levels (Fig. S4) further supported the fast-to-slow transition detected in the skeletal muscles of the ALS animal model by the proteomic approach presented here.

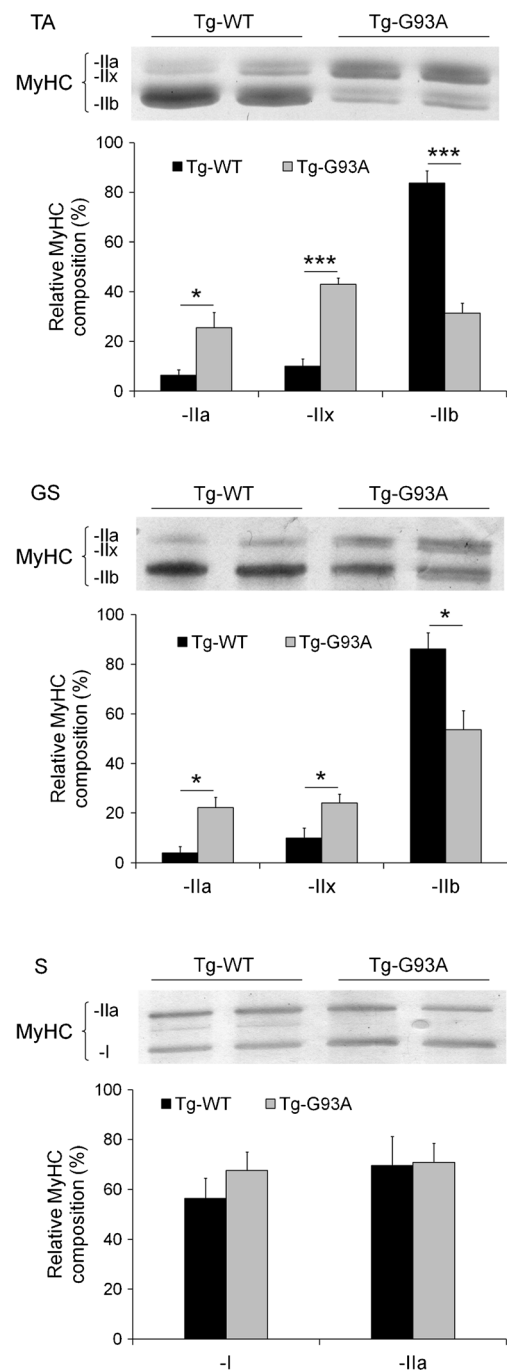
Discussion

Establishing the exact pattern of MyHC isoforms is an important issue in diverse areas of muscular pathophysiology. Thus far, this type of study has mainly used conventional gel-based or (immuno)histochemistry tools, which, however, suffer from disadvantages such as lack of accuracy, poor reproducibility, and exceedingly long execution times.

To overcome these limitations, we have developed a targeted mass spectrometry approach that uses SRM for the absolute quantification of different MyHC isoforms. This protocol can be performed easily and in a relatively short time, and allows the collection of data from a large number of samples with high reproducibility [51].

We verified the latter aspect with regard to MyHC quantification in three distinct analyses of a single muscle sample, finding that the average CV was less than 10%. Importantly, as also reported here, the SRM-based technology offers the advantage to measure absolute values for MyHC expression in different muscles, or in the same muscle under different conditions.

With the specific aim of verifying the use of the technique for diagnostic purposes, we investigated whether the SRM-based approach could identify MyHC alterations in an ALS Tg mouse model, in light of previous suggestions of an active role of skeletal muscle alterations in ALS pathogenesis



[34–36]. This study, performed in terminally ill Tg-G93A mice (already proven to closely mimic human skeletal myofiber alterations during early disease manifestation [15]) and age-matched healthy mice not only proved the applicability of the procedure but also revealed new insights in ALS-linked muscle alterations.

In particular, we found alterations in some, but not all, skeletal muscles examined, as fast tibialis anterior and gastrocnemius muscles displayed reduced expression of the very fast twitch type IIb MyHC isoform, and there was concomitant

Fig. 5 SDS-PAGE analyses confirm the MyHC shift in the tibialis anterior (TA) and gastrocnemius (GS) muscles of Tg-G93A mice compared with Tg-WT mice. The same tibialis anterior (upper panel), gastrocnemius (middle panel), and soleus (S; lower panel) samples analyzed by SRM (reported in Fig. 4) were subjected to SDS-PAGE protein separation followed by silver staining of gels. The upper part of each panel shows silver-stained MyHCs from two of three different biological replicates. The lower part of each panel, which reports the densitometric analysis of MyHC bands, confirms the SRM-highlighted MyHC shift from type IIb to type IIa and type IIx in the tibialis anterior and gastrocnemius muscles (but not in the soleus muscle) of terminally ill amyotrophic lateral sclerosis mice compared with healthy counterparts. The values are the mean \pm SEM, $n = 3$; other experimental details are as in the legend for Fig. 4. One asterisk $p < 0.05$, three asterisks $p < 0.005$, Student's t test

increased expression of the moderately fast type IIa and type IIx MyHC isoforms. Conversely, whereas the other fast muscle, extensor digitorum longus muscle, showed a similar trend that, however, could not be statistically confirmed, no difference was observed in mixed (i.e., diaphragm) or slow (i.e., soleus) muscles. These findings are in agreement with those previously reported in younger ALS mice, indicating a selective loss of

the fast-twitch fiber-containing, and most forceful, motor units, which is partially compensated by a transition toward slower, and less forceful, motor units [15, 52].

The preferential loss of fast-twitch fibers may be caused by the selective vulnerability of fast-fatiguable, and fast fiber-innervating, motor neurons that—in *SOD1* ALS mouse models—undergo axonal degeneration long before the appearance of symptoms [53, 54]. Concomitantly, the progressive muscle atrophy [35] and non-autonomous motor neuron degeneration [34], which were observed in Tg mice expressing the *SOD1* mutant only in skeletal muscles, suggest that skeletal muscle alterations are primary events in ALS pathogenesis, and that muscle-to-nerve back-signaling may contribute to motor neuron disease. In light of this information, it is possible that the robustness, reproducibility, and rapidity of the proposed SRM-based method will allow analysis of the with-time variation of MyHC expression patterns in pre-symptomatic, symptomatic, and end-stage ALS animal models and in postdiagnosis humans, as well as serving as a basis for development of novel diagnostic/prognostic tools of (neuro)muscular diseases.

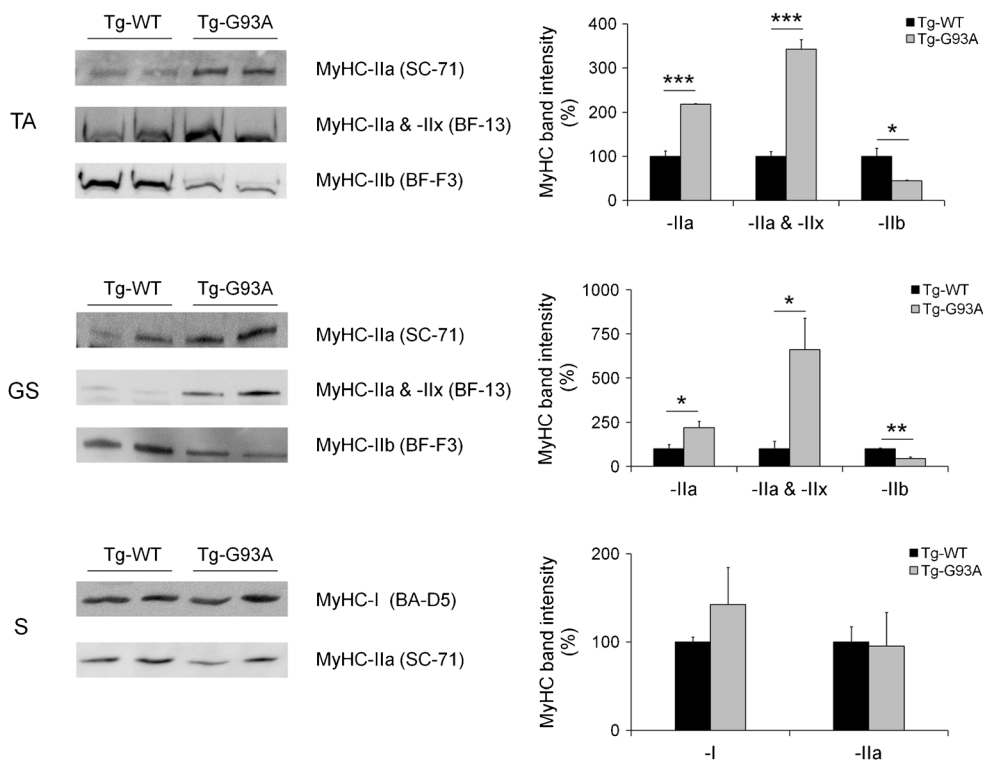


Fig. 6 Western blot studies confirm the MyHC fast-to-slow shift in the tibialis anterior (TA) and gastrocnemius (GS) muscles of Tg-G93A mice compared with Tg-WT mice. After protein separation by SDS-PAGE, the same muscle protein samples of tibialis anterior (upper panel), gastrocnemius (middle panel) and soleus (S; lower panel) muscles used in the experiments reported in Figs. 4 and 5, were analyzed by Western blot after SDS-PAGE protein separation, with use of monoclonal antibodies to type IIa MyHC (clone SC-71), type IIb MyHC (clone BF-F3), and both type IIa and type IIx MyHC (clone BF-13). Western blots of

two of three different biological replicates for the different MyHCs in each of the muscles analyzed are shown on the left. The densitometric analyses of MyHC immunoreactive bands, reported as a percentage of the content of each MyHC in Tg-WT muscles, are shown on the right. The data obtained are in agreement with those obtained by both the SRM-based quantification and the analysis of silver-stained gels. The reported values are the mean \pm SEM, $n = 3$. One asterisk $p < 0.05$, two asterisks $p < 0.01$, three asterisks $p < 0.005$, Student's t test

Acknowledgements This work was supported by grants from the AriSLA Foundation (project LoCaLS 2013 to A.B.) and the University of Padua (PRAT CPDA121988/12 to M.C.S. and PRAT CPDA158035/15 to A.B.). The authors thank Giorgio Arrigoni and Marta Murgia (Department of Biomedical Science, University of Padua) for helpful discussions and advice.

Compliance with ethical standards

Conflict of interest The authors declared that they have no conflict of interest.

References

- Dubowitz V, Pearse AG. Reciprocal relationship of phosphorylase and oxidative enzymes in skeletal muscle. *Nature*. 1960;185:701–2.
- Edström L, Kugelberg E. Histochemical composition, distribution of fibres and fatigability of single motor units. Anterior tibial muscle of the rat. *J Neurol Neurosurg Psychiatry*. 1968;31:424–33.
- Stein JM, Padikula HA. Histochemical classification of individual skeletal muscle fibers of the rat. *Am J Anat*. 1962;110:103–23.
- Brooke MH, Kaiser KK. Three “myosin adenosine triphosphatase” systems: the nature of their pH lability and sulfhydryl dependence. *J Histochem Cytochem*. 1970;18:670–2.
- Reggiani C, Bottinelli R, Stienen GJ. Sarcomeric myosin isoforms: fine tuning of a molecular motor. *News Physiol Sci*. 2000;15:26–33.
- Pette D, Staron RS. Cellular and molecular diversities of mammalian skeletal muscle fibers. *Rev Physiol Biochem Pharmacol*. 1990;116:1–76.
- Schiaffino S, Reggiani C. Molecular diversity of myofibrillar proteins: gene regulation and functional significance. *Physiol Rev*. 1996;76:371–423.
- Rossi AC, Mammucari C, Argentini C, Reggiani C, Schiaffino S. Two novel/ancient myosins in mammalian skeletal muscles: MYH14/7b and MYH15 are expressed in extraocular muscles and muscle spindles. *J Physiol*. 2010;588:353–64.
- Staron RS, Pette D. Correlation between myofibrillar ATPase activity and myosin heavy chain composition in rabbit muscle fibres. *Histochemistry*. 1986;86:19–23.
- McLoon LK, Park HN, Kim JH, Pedrosa-Domellöf F, Thompson LV. A continuum of myofibers in adult rabbit extraocular muscle: force, shortening velocity, and patterns of myosin heavy chain colocalization. *J Appl Physiol*. 2011;111:1178–89.
- Stephenson GM. Hybrid skeletal muscle fibres: a rare or common phenomenon? *Clin Exp Pharmacol Physiol*. 2001;28:692–702.
- Harrison BC, Allen DL, Leinwand LA. IIb or not IIb? Regulation of myosin heavy chain gene expression in mice and men. *Skelet Muscle*. 2011;1:5.
- Blaauw B, Schiaffino S, Reggiani C. Mechanisms modulating skeletal muscle phenotype. *Compr Physiol*. 2013;3:1645–87.
- Webster C, Silberstein L, Hays AP, Blau HM. Fast muscle fibers are preferentially affected in Duchenne muscular dystrophy. *Cell*. 1988;52:503–13.
- Hegedus J, Putman CT, Tyreman N, Gordon T. Preferential motor unit loss in the SOD1 G93A transgenic mouse model of amyotrophic lateral sclerosis. *J Physiol*. 2008;586:3337–51.
- Dobrowolny G, Aucello M, Musarò A. Muscle atrophy induced by SOD1G93A expression does not involve the activation of caspase in the absence of denervation. *Skelet Muscle*. 2011;1:3.
- Clarke NF. Congenital fiber-type disproportion. *Semin Pediatr Neurol*. 2011;18:264–71.
- Tajsharghi H, Oldfors A. Myosinopathies: pathology and mechanisms. *Acta Neuropathol*. 2013;125:3–18.
- Brooke MH, Kaiser KK. Three “myosin ATPase” systems. The nature of their pH lability and sulphhydryl dependence. *J Histochem Cytochem*. 1970;18:670–2.
- Khan MA. Histochemical sub-types of three fibre-types of avian skeletal muscle. *Histochemistry*. 1976;50:9–16.
- Staron RS, Hikida RS. Histochemical, biochemical, and ultrastructural analyses of single human muscle fibers, with special reference to the C-fiber population. *J Histochem Cytochem*. 1982;40:563–8.
- Schiaffino S, Gorza L, Sartore S, Saggin L, Ausoni S, Vianello M, et al. Three myosin heavy chain isoforms in type 2 skeletal muscle fibres. *J Muscle Res Cell Motil*. 1989;10:197–205.
- Talmadge RJ, Roy RR. Electrophoretic separation of rat skeletal muscle myosin heavy-chain isoforms. *J Appl Physiol*. 1993;75:2337–40.
- Bamman MM, Clarke MS, Talmadge RJ, Feeback DL. Enhanced protein electrophoresis technique for separating human skeletal muscle myosin heavy chain isoforms. *Electrophoresis*. 1999;20:466–8.
- Blough ER, Rennie ER, Zhang F, Reiser PJ. Enhanced electrophoretic separation and resolution of myosin heavy chains in mammalian and avian skeletal muscles. *Anal Biochem*. 1996;233:31–5.
- Sant’Ana Pereira JA, Greaser M, Moss RL. Pulse electrophoresis of muscle myosin heavy chains in sodium dodecyl sulfate-polyacrylamide gels. *Anal Biochem*. 2001;291:229–36.
- Picard B, Barboiron C, Chadeyron D, Jurie C. Protocol for high-resolution electrophoresis separation of myosin heavy chain isoforms in bovine skeletal muscle. *Electrophoresis*. 2011;32:1804–6.
- Mizunoya W, Wakamatsu J, Tatsumi R, Ikeuchi Y. Protocol for high-resolution separation of rodent myosin heavy chain isoforms in a mini-gel electrophoresis system. *Anal Biochem*. 2008;377:111–3.
- Cleveland DW, Rothstein JD. From Charcot to Lou Gehrig: deciphering selective motor neuron death in ALS. *Nat Rev Neurosci*. 2001;2:806–19.
- Rowland LP, Schneider NA. Amyotrophic lateral sclerosis. *N Engl J Med*. 2001;344:1688–700.
- Rosen DR, Siddique T, Patterson D, Figlewicz DA, Sapp P, Hentati A, et al. Mutations in Cu/Zn superoxide dismutase gene are associated with familial amyotrophic lateral sclerosis. *Nature*. 1993;362:59–62.
- Gurney ME, Pu H, Chiu AY, Dal Canto MC, Polchow CY, Alexander DD, et al. Motor neuron degeneration in mice that express a human Cu, Zn superoxide dismutase mutation. *Science*. 1994;264:1772–5.
- Ferri A, Nencini M, Casciati A, Cozzolino M, Angelini DF, Longone P, et al. Cell death in amyotrophic lateral sclerosis: interplay between neuronal and glial cells. *FASEB J*. 2004;18:1261–3.
- Wong M, Martin LJ. Skeletal muscle-restricted expression of human SOD1 causes motor neuron degeneration in transgenic mice. *Hum Mol Genet*. 2010;19:2284–302.
- Dobrowolny G, Aucello M, Rizzuto E, Beccafico S, Mammucari C, Boncompagni S, et al. Skeletal muscle is a primary target of SOD1G93A-mediated toxicity. *Cell Metab*. 2008;8:425–36.
- Pansarasa O, Rossi D, Berardinelli A, Cereda C. Amyotrophic lateral sclerosis and skeletal muscle: an update. *Mol Neurobiol*. 2014;49:984–90.
- Stella R, Massimino ML, Sandri M, Sorgato MC, Bertoli A. Cellular prion protein promotes regeneration of adult muscle tissue. *Mol Cell Biol*. 2010;30:4864–76.
- Massimino ML, Peggion C, Loro F, Stella R, Megighian A, Scorzeto M, et al. Age-dependent neuromuscular impairment in prion protein knock-out mice. *Muscle Nerve*. 2016;53:269–79.

39. Switzer RC, Merrill CR, Shifrin S. A highly sensitive silver stain for detecting proteins and peptides in polyacrylamide gels. *Anal Biochem.* 1979;98:231–7.
40. Wiśniewski JR, Zougman A, Nagaraj N, Mann M. Universal sample preparation method for proteome analysis. *Nat Methods.* 2009;6:359–62.
41. Kirkpatrick DS, Gerber SA, Gygi SP. The absolute quantification strategy: a general procedure for the quantification of proteins and post-translational modifications. *Methods.* 2005;35:265–73.
42. MacLean B, Tomazela DM, Shulman N, Chambers M, Finney GL, Frewen B, et al. Skyline: an open source document editor for creating and analyzing targeted proteomics experiments. *Bioinformatics.* 2010;26:966–8.
43. Karlsson C, Malmström L, Aebersold R, Malmström J. Proteome-wide selected reaction monitoring assays for the human pathogen *Streptococcus pyogenes*. *Nat Commun.* 2012;3:1301.
44. Picotti P, Rinner O, Stallmach R, Dautel F, Farrah T, Domon B, et al. High-throughput generation of selected reaction-monitoring assays for proteins and proteomes. *Nat Methods.* 2010;7:43–6.
45. Wolf-Yadlin A, Hautaniemi S, Lauffenburger DA, White FM. Multiple reaction monitoring for robust quantitative proteomic analysis of cellular signalling networks. *Proc Natl Acad Sci U S A.* 2007;104:5860–5.
46. Lange V, Picotti P, Domon B, Aebersold R. Selected reaction monitoring for quantitative proteomics: a tutorial. *Mol Syst Biol.* 2008;4:222.
47. Mallick P, Schirle M, Chen SS, Flory MR, Lee H, Martin D, et al. Computational prediction of proteotypic peptides for quantitative proteomics. *Nat Biotechnol.* 2007;25:125–31.
48. Holman SW, Sims PF, Eyers CE. The use of selected reaction monitoring in quantitative proteomics. *Bioanalysis.* 2012;4:1763–8.
49. Murgia M, Nagaraj N, Deshmukh AS, Zeiler M, Cancellara P, Moretti I, et al. Single muscle fiber proteomics reveals unexpected mitochondrial specialization. *EMBO Rep.* 2015;16:387–95.
50. Hughes SM, Taylor JM, Tapscott SJ, Gurley CM, Carter WJ, Peterson CA. Selective accumulation of MyoD and myogenin mRNAs in fast and slow adult skeletal muscle is controlled by innervation and hormones. *Development.* 1993;118:1137–47.
51. Picotti P, Aebersold R. Selected reaction monitoring-based proteomics: workflows, potential, pitfalls and future directions. *Nat Methods.* 2012;9:555–66.
52. Hegedus J, Putman CT, Gordon T. Time course of preferential motor unit loss in the SOD1 G93A mouse model of amyotrophic lateral sclerosis. *Neurobiol Dis.* 2007;28:154–64.
53. Pun S, Santos AF, Saxena S, Xu L, Caroni P. Selective vulnerability and pruning of phasic motoneuron axons in motoneuron disease alleviated by CNTF. *Nat Neurosci.* 2006;9:408–19.
54. Saxena S, Roselli F, Singh K, Leptien K, Julien JP, Gros-Louis F, et al. Neuroprotection through excitability and mTOR required in ALS motoneurons to delay disease and extend survival. *Neuron.* 2013;80:80–96.